Pulsed Laser Ablation of Sn and SnO_2 Targets: Neutral Composition, Energetics, and Wavelength Dependence

Scott A. Reid,*,† Wei Ho,† and F. J. Lamelas‡

Department of Chemistry and Department of Physics, Marquette University, P.O. Box 1881, Milwaukee, Wisconsin 53201-1881

Received: January 31, 2000; In Final Form: March 27, 2000

We report time-of-flight mass spectrometric studies of neutral gas-phase species generated in 532 and 355 nm laser ablation of Sn and SnO_2 targets at intensities of $\approx 10^8$ W cm^{-2}, below the plasma threshold. A wavelength-dependent yield of Sn:Sn_xO_y species is observed for the oxide target, with Sn_xO_x ($x = 1-3$) the primary products at 532 nm and atomic Sn dominant at 355 nm. Sn and Sn_2 are the primary products of Sn metal ablation, and the relative Sn:Sn_2 yield increases at the shorter wavelength. The speed distributions of neutrals ejected from the oxide target are well represented by unshifted time-transformed Maxwell−Boltzmann (MB) distributions, while those ejected from the metal target exhibit bimodal MB distributions. Typical most-probable speeds are $(1-2) \times 10^5$ cm s^{-1}, with peak kinetic energies (KEs) of 1−2 eV. The implications of our results for pulsed laser deposition of SnO_x films will be emphasized.

I. Introduction

Thin-film materials based on optically transparent semiconductors have important applications as gas sensors, in display systems, and in solar cells.[1−5] The n-type semiconductor SnO_2 is a promising base material for such devices. Thin polycrystalline SnO_2 films exhibit high sensitivity to a variety of gases, and doping can improve selectivity.[6−10] Film sensitivity is increased for average grain sizes $\langle D \rangle$ comparable to the length of the space charge region L, which is typically several nanometers.[11] When $\langle D \rangle < 2L$, entire grains are electron depleted and an increase in gas sensitivity is expected.[11] Thin films exhibiting $\langle D \rangle < 5$ nm, comparable to $2L$, have recently been grown using pulsed laser deposition (PLD).[12] This is but one of several recent reports of PLD-generated SnO_x films that have utilized a variety of substrates, targets, and deposition conditions.[12−19] The as-grown films range from polycrystalline[13,16] to amorphous[12,19] in structure and with O:Sn stoichiometries ranging from near 2:1[16] to <1:1.[13,19] Very recently, we produced the high-pressure o-SnO_2 phase in high (∼50%) yield from postdeposition heat treatment of initially amorphous films of near 1:1 O:Sn stoichiometry.[19]

The variability in results obtained for PLD-generated SnO_x films illustrates a sensitivity to growth process variables and underscores the importance of characterizing the composition and energetics of products ablated from Sn-containing targets at intensities typical of deposition. We recently reported the first study for an SnO_2 target, applying time-of-flight mass spectrometry (TOFMS) to analyze the neutral products of ablation at 532 nm.[20] In this paper we examine neutrals produced in 532 and 355 nm ablation of Sn and SnO_2 targets at intensities of 10^8 W cm^{-2}, near but below the ablation threshold for both targets. Our goal is to understand the mechanism(s) of the initial laser−target interaction and correlate the properties of PLD-generated SnO_x films with growth process variables.

Over the past 30 years, a variety of thin-film materials have been fabricated using PLD[21] and many studies of laser ablation have been reported. The ablation threshold is associated with formation of a dense plume or plasma above the target surface and the onset of gas-dynamic effects, which occur for material ejection rates exceeding 0.1−1 monolayer per pulse. In PLD nomenclature, this threshold delineates regimes of incongruent and congruent (i.e., stoichiometric) material transfer.[22] The latter arises from nonthermal target erosion characteristic of a laser-generated plasma. Early studies of nanosecond ablation typically invoked a transient surface heating mechanism, based on expected thermalization times that are short compared to the laser pulse duration. Recent studies have shown the importance of electronic effects,[23] and for semiconductors a parameter important in governing these effects is the ratio of photon ($h\nu$) to band-gap (E_{gap}) energies. Supragap excitation ($h\nu > E_{gap}$) involves single photon band-to-band transitions in the bulk solid as well as transitions among surface states,[24] while subgap excitation primarily involves transitions at localized defect states, except at high intensities where multiphoton band-to-band transitions contribute. Studies of photon energy dependencies such as reported here are important in characterizing relative contributions from thermal vs electronic processes. In the ablation regime, secondary electronic processes including formation of a laser-induced plasma, ionization of emitted neutral species, and photoabsorption by free electrons will also contribute.[22−24] Here we focus on a intensity regime near but below the plasma threshold, but will also report initial results concerning laser intensity dependencies.

The outline of the paper is as follows. Section II is a summary of the experimental methodology. Sections IIIa and IIIb include our results for ablation of Sn and SnO_2 targets at wavelengths of 532 and 355 nm and intensities of $\approx 10^8$ W cm^{-2}. These wavelengths correspond to photon energies well below and near, respectively, the 3.5 eV band gap of SnO_2.[13] A discussion of these results, focusing on the laser−target interaction and implications for PLD studies, is provided in section IIIC. Our conclusions are summarized in section IV.

* To whom correspondence should be addressed. E-mail: scott.reid@marquette.edu.
† Department of Chemistry.
‡ Department of Physics.

10.1021/jp000369a CCC: $19.00
Published on Web 05/06/2000

II. Experimental Section

A diagram of the experimental apparatus was given in ref 20. Pulsed Nd:YAG lasers (Continuum NY-61, Surelite II) were used for ablation and ionization. Typical ablation pulse energies were 1−5 mJ in a 6−8 ns pulse (fwhm). The beam struck the target along the surface normal, with a spot size of 1 mm. The beam area at the target was estimated using burn paper, and calculated intensities are based on a "top-hat" spatial profile. The ablated material passed into the interaction region of a linear time-of-flight mass spectrometer (TOFMS) and was ionized by 118.2 nm photons generated by tripling 10 mJ of the 355 nm output of the second Nd:YAG system in a cell filled with 0.8 mbar of Xe. The separation d between target and ionization region was fixed at 70 ± 1 mm for the oxide target and 73 ± 1 mm for the metal target. Following extraction and acceleration, the ions traversed a distance of 118 cm before striking a dual microchannel plate detector. The signal was amplified (×25) using a fast preamplifier (Stanford Research 445) and recorded by a multichannel scaler (SR 430) with 5 ns bin width. The ablation laser Q-switch was triggered at half the rate of the ionization laser, allowing active background subtraction. Timing of ablation and ionization laser Q-switch triggers was set using a digital delay generator (SR DG535). The mass spectrometer had a typical resolution ($m/\Delta m$) of ∼200 at a mass of 120 amu.

Two types of data will be reported. The first type is mass spectra accumulated over typically 5000 ablation laser shots at a set ablation−ionization laser delay, or neutral arrival time. These spectra give the relative neutral distribution at a fixed arrival time, or speed determined by the separation d between target and ionization region. The second type of data to be reported is the arrival-time (speed) distributions of mass-selected species, obtained by varying the ablation−ionization laser delay and accumulating mass spectra over 5000 shots at each delay setting. Intensity fluctuations over the course of an experiment were corrected for by normalizing to spectra repetitively acquired at a reference delay near the peak of the Sn arrival-time distribution.

The SnO_2 targets were prepared by cold pressing approximately 10 g of SnO_2 powder (Aldrich, >99.9%) into a 0.75'' long by 0.5'' diameter pellet at a typical pressure of 6000 psi. The pellets were annealed for 60−70 h at 1473 K prior to use. The Sn target (Aldrich, 6 mm diameter rod, 99.99%) was polished with a fine (typically 400) grit paper and cleaned with acetone prior to use. A motorized, computer-controlled linear-rotary motion feed through was used to simultaneously translate and rotate the target. During experiments the main chamber and flight tube pressures were 3×10^{-7} and 10^{-7} mbar, respectively.

III. Results and Discussion

A. Laser Ablation of SnO_2 at 532 and 355 nm. We first examined the 532 nm ablation of an SnO_2 target. Figure 1 displays a mass spectrum obtained at a pulse energy of 5 mJ, or intensity of approximately 10^8 W cm^{-2}, and neutral arrival time of 65 μs. The background arises from ablated ions, is integrated over all arrival times, species, and states, and thus is not indicative of the true ion fraction. It is most pronounced at the beginning of a given experiment, as is the neutral signal from surface impurities, primarily the alkali metals Na, K, and Ca. The presence of these impurities is attributed to their high volatility, low ionization potentials (IPs), and presence on the surface in ionic compounds.[25]

The signal observed for Sn-containing compounds is dominated by SnO and Sn_2O_2. Smaller signals are observed for Sn, Sn_3O_3, and the hypermetallic[26] compound Sn_2O. Gas-phase

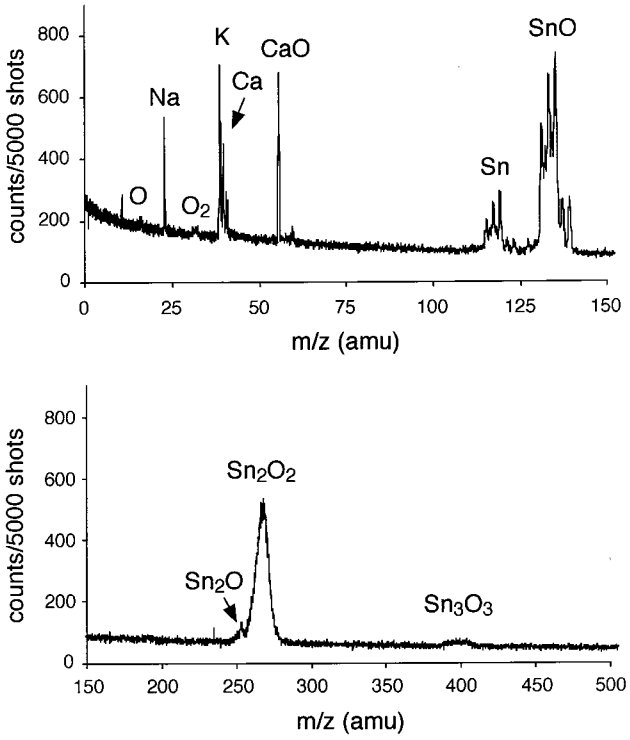

Figure 1. Mass spectrum of the neutral products of 532 nm pulsed laser ablation of an SnO_2 target.

SnO_2 is not detected. The IPs of both O (13.64 eV)[27] and O_2 (12.071 eV)[27] lie above our ionizing photon energy (10.49 eV), and the observed signals probably arise from secondary (electron impact) ionization. We note that gas-phase Sn_xO_x ($x = 1-8$) has previously been observed in equilibrium above heated SnO_2 samples[28] and oxygen saturated tin melts.[29]

Figure 2 displays the integrated mass counts (points) as a function of neutral arrival time for Sn, SnO, and Sn_2O_2. We fit the arrival-time distributions shown in Figure 2 to unshifted time-transformed Maxwell−Boltzmann (MB) speed distributions of the form[30]

$$S(t) = (A/d^3)(t_{peak}/t)^4 \exp\{-2(t_{peak}/t)^2\} \quad (1)$$

In eq 1, d is the target−ionization region separation, t_{peak} is the maximum in the arrival-time distribution, and A is a scaling constant. Nonlinear least-squares fits to eq 1 give most-probable speeds of 1.7×10^5 cm s^{-1} (Sn), 1.4×10^5 cm s^{-1} (SnO), and 1.2×10^5 cm s^{-1} (Sn_2O_2), or peak kinetic energies (KEs) of 1.8, 1.4, and 2.0 eV. The estimated uncertainty in all most-probable speeds and KEs reported is $\pm 2 \times 10^4$ cm s^{-1} and ±0.1 eV, respectively. Temperature values of 1.1×10^4 K (Sn), 7.8×10^3 K (SnO), and 1.1×10^4 K (Sn_2O_2) are obtained.

We also fit our data to a shifted Maxwellian distribution, which describes the speed distribution of molecules in a supersonic jet[31] and has been used to model particle speed distributions in laser ablation.[32−36] The time-transformed distribution has the form[33]

$$S(t) = At^{-4} \exp\{-c_1 t^{-2} + c_2 t^{-1}\} \quad (2)$$

where $c_1 = md/(2kT)$, m is the molecular mass, T is the absolute temperature, and $c_2 = 2c_1u/d$, where u is the stream velocity. The fits obtained to this distribution were of a quality similar to those obtained using eq 1, with similar derived temperatures and near-zero stream velocities ($u \approx 0$). We therefore report fit parameters only for the unshifted distribution (eq 1).

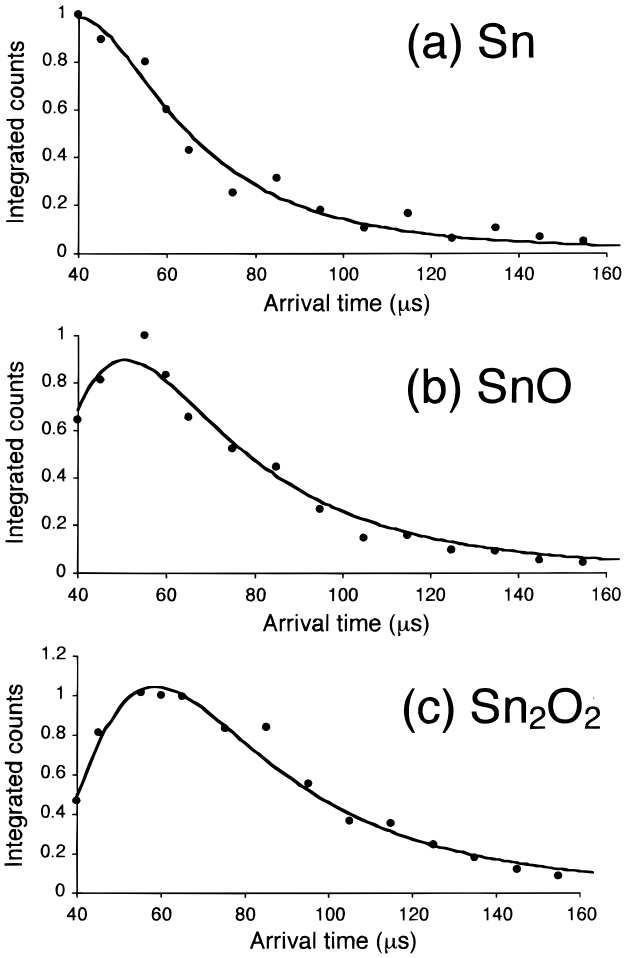

Figure 2. Arrival-time distributions (points) for (a) Sn, (b) SnO, and (c) Sn_2O_2 from 532 nm ablation of an SnO_2 target. The lines are fits to an unshifted time-transformed Maxwell−Boltzmann speed distribution, from which the most probable speed, peak kinetic energy, and temperature were derived.

We estimated relative species abundances by integrating the fits to eq 1. SnO and Sn_2O_2 fragmentation to Sn and SnO, respectively, was negligible in the ionization step (<5%).[20] Relative Sn:SnO:Sn_2O_2 abundances of 0.22:0.65:1.0 are obtained under the assumption of similar photoionization efficiencies, which is questionable. The IP of Sn_2O_2 is unknown, while that of SnO (10.5 ± 0.5 eV)[27] lies close to the ionizing photon energy of 10.49 eV and is far above that of Sn (7.344 eV).[27] Intensity calibration would require knowledge of vacuum ultraviolet absorption cross sections and ionization quantum yields, yet important relative trends may still be identified, e.g., the dependence of neutral composition on laser intensity and wavelength.

Figure 3 displays the neutral signal dependence on laser pulse energy in the range 2.1−20.1 mJ, corresponding to intensities of approximately $5 \times 10^7 - 5 \times 10^8$ W cm^{-2}. The signal increases exponentially at low pulse energies (<8 mJ pulse^{-1}) and then flattens. We observed similar behavior for the Sn target, and in that case the break in the curve correlates with the onset of visible emission from atomic neutrals and ions, and occurs at a fluence similar to the reported ablation threshold at 248 nm.[37] We therefore correlate this point with the onset of ablation, an assumption supported by estimates of the neutral angular dependence determined via the thickness distribution of SnO films grown on Si(001) substrates using 532 nm PLD at a pulse energy of 10 mJ. The as-grown films exhibit an elliptical interference pattern, the shape arising from the laser spatial

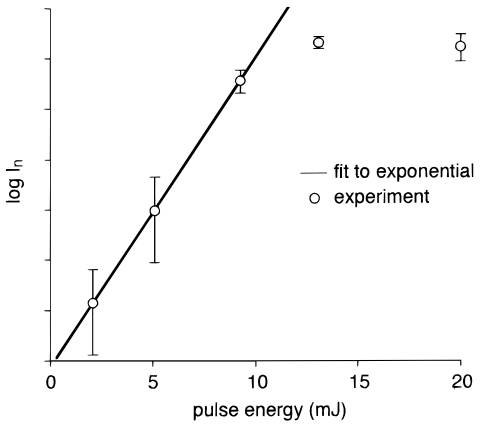

Figure 3. Pulse energy dependence of the total yield of neutral Sn-containing species for 532 nm ablation of an SnO_2 target.

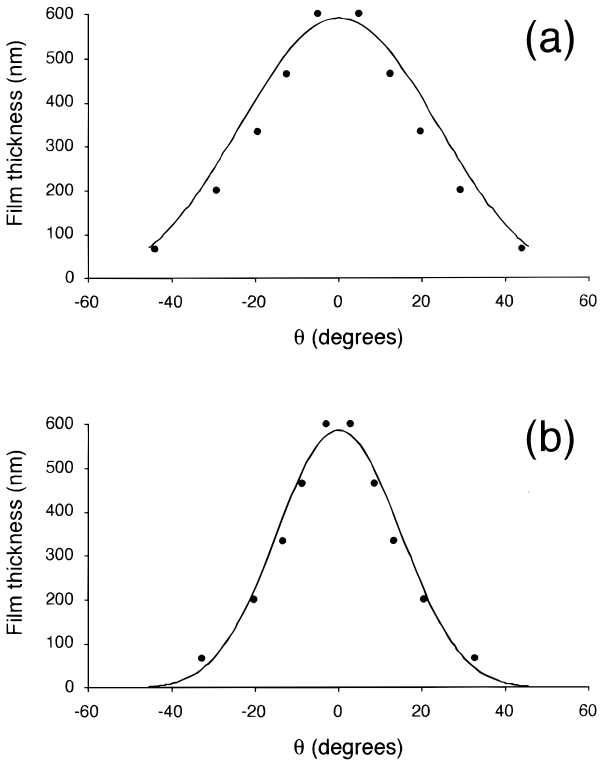

Figure 4. Thickness distribution for SnO_x ($x \approx 1$) films grown using 532 nm PLD from an SnO_2 target. Distributions were determined by analyzing interference fringes, as described in the text, and are given (points) for cuts along (a) semimajor and (b) semiminor axes of the elliptically patterned film. The lines in each figure represent fits to a $\cos^{n+3}\theta$ distribution, from which sharpness parameters (n) of (a) 6 and (b) 15 were derived.

profile, and Figure 4 displays thickness distributions for cuts along the semimajor and semiminor axes. These distributions were determined from the interference fringes using the equation[38]

$$2t = (m + 1/2)\lambda_n \tag{3}$$

where $m = 0, 1, 2, \ldots$ and $\lambda_n = \lambda_0/n$. In our analysis n was taken as 1.5, and the violet fringes were used and λ_0 was therefore taken as 400 nm. Given an angular flux distribution of form $\cos^n \theta$, where n is the sharpness parameter, the distributions can be represented by the following equation:[39]

$$D(\theta) = A \cos^{n+3}\theta \tag{4}$$

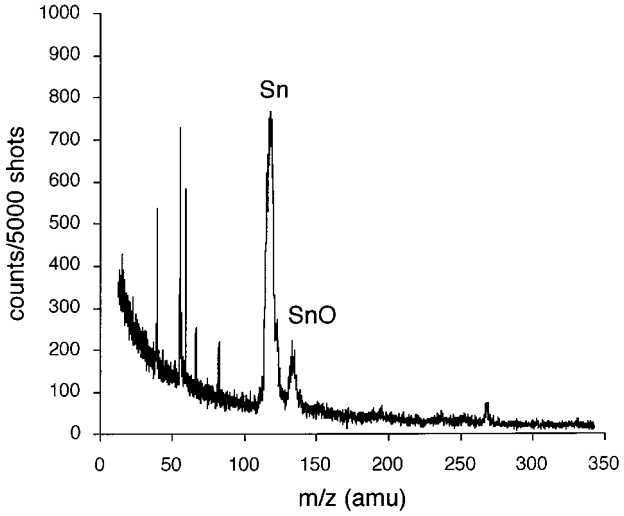

Figure 5. Mass spectrum of the neutral products of 355 nm ablation of an SnO_2 target. Note the relative increase in the ratio of signals for $Sn:Sn_xO_y$ species compared to ablation at 532 nm (Figure 1).

The fits to eq 4 are shown as solid lines in Figure 4, and from these fits n values of 6 ± 1 and 15 ± 2 are obtained for the semimajor and semiminor axis distributions, respectively. These values are significantly larger than expected in a thermal regime ($n = 1$) and are consistent with the presence of gas-dynamic effects.

The photon-energy dependence of the ablation products was investigated by collecting a second set of data using a wavelength of 355 nm. Figure 5 displays the mass spectrum obtained at a pulse energy of 2.5 mJ, or intensity of approximately 5×10^7 W cm^{-2}, and neutral arrival time of 40 μs. Marked changes in peak intensities and an increased background are observed compared to ablation at 532 nm (Figure 1). A lower pulse energy was used here to reduce the background signal, yet our preliminary fluence dependence studies show that the neutral composition and energetics vary little between 2.5 and 5 mJ. Hence the differences between Figures 1 and 5 cannot be attributed to this factor. The arrival-time distributions at 355 nm are still well described by a single-component MB distribution. The Sn and SnO distributions (points) and fits to eq 1 (lines) are shown in parts a and b, respectively, Figure 6. Most-probable speeds of 2.2×10^5 cm s^{-1} (Sn) and 1.7×10^5 cm s^{-1} (SnO), peak KEs of 3.0 and 2.0 eV, and temperatures of 1.8×10^4 and 1.2×10^4 K, respectively, are obtained. The relative Sn:SnO abundance is 5.2:1.0, an increase of approximately 15 times compared to ablation at 532 nm. Comparing the relative yield of Sn to all tin oxide species, i.e., $Sn:Sn_xO_y$, the increase is approximately 40 times.

B. Laser Ablation of Sn at 532 and 355 nm. We conducted a similar set of experiments for the Sn target at intensities of approximately half the ablation threshold. Figure 7 displays the mass spectrum obtained following 532 nm ablation of the Sn target at 2.1 mJ pulse^{-1}, corresponding to a intensity of approximately 5×10^7 W cm^{-2}, and neutral arrival time of 55 μs. The primary Sn-containing compounds observed are of form Sn_x ($x = 1-3$), with intensities that decrease with increasing x. Figure 8 displays nonlinear least-squares fits of the observed mass peaks for Sn and Sn_2 based on natural abundance isotopic distributions,[27] with the width and overall intensity used as fit parameters.

The arrival-time distributions and relative abundances were investigated. The Sn and Sn_2 distributions were not well fit by single-component MB distributions, but were better represented

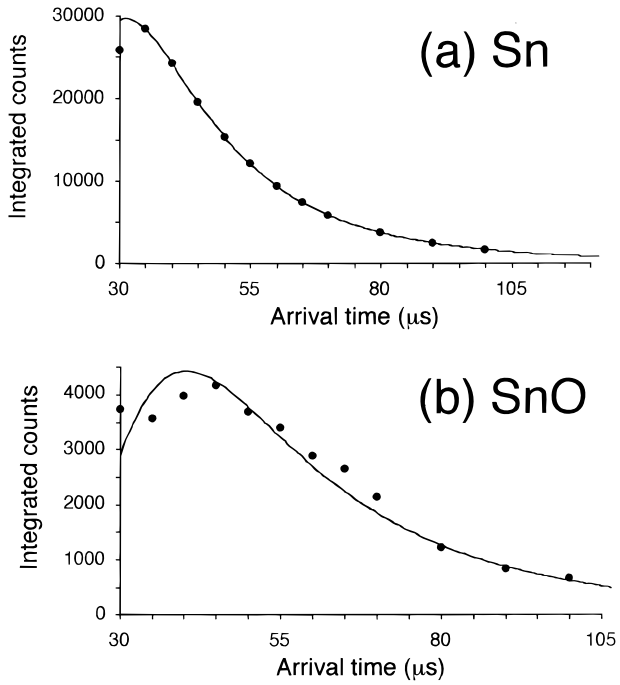

Figure 6. Arrival-time distributions (points) for (a) Sn and (b) SnO following 355 nm ablation of an SnO_2 target. The lines in each plot are fits to an unshifted time-transformed Maxwell−Boltzmann speed distribution.

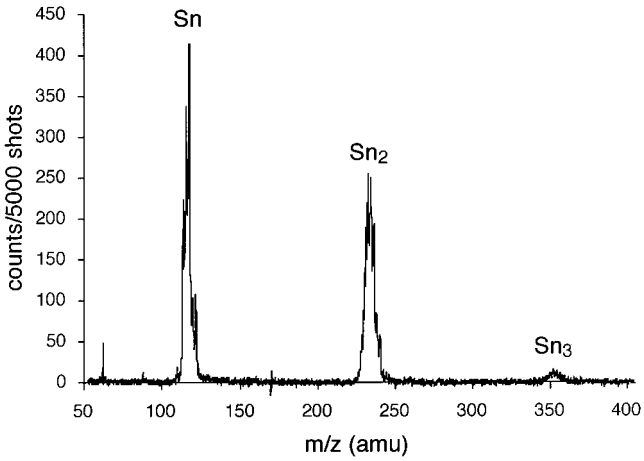

Figure 7. Mass spectrum of the neutral products of 532 nm pulsed laser ablation of a Sn target.

by two-component distributions with a dominant fast component and weak slow component peaking near 110 μs. The data and fits for Sn and Sn_2 are shown in Figure 9. For Sn, the fit gave t_{peak} values of 44.7 and 115.9 μs for the two components and a ratio of fast to slow component of ≈5:1. The primary (fast) component corresponds to a most-probable speed of 1.6×10^5 cm s^{-1} or peak KE of 1.7 eV and a temperature of 1.1×10^4 K. The Sn_2 fit gave t_{peak} values of 55.5 and 107 μs and ratio of fast to slow component of ≈3:1. The primary component corresponds to a most-probable speed of 1.3×10^5 cm s^{-1} or peak KE of 1.8 eV and a temperature of 1.1×10^4 K. We estimated the relative abundance using the integrated fits and find a $Sn:Sn_2$ ratio of 1.4:1.0 under the assumption of similar photoionization efficiencies.

Figure 10 displays the mass spectrum obtained at a neutral arrival time of 50 μs following 355 nm ablation of the Sn target at a pulse energy of 1.2 mJ or intensity of approximately 3×10^7 W cm^{-2}. The relative cluster signal is reduced and a higher background is observed. The Sn distribution was fit to a two-

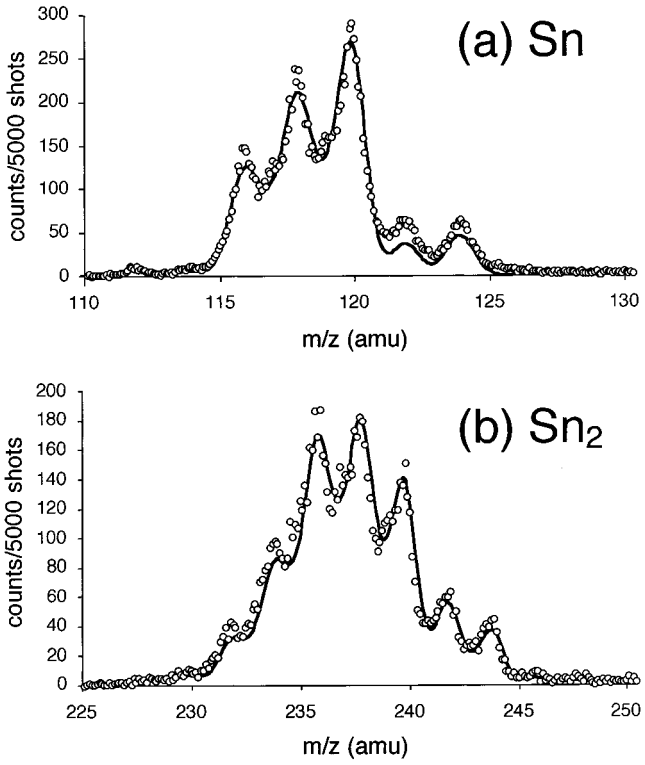

Figure 8. Time-of-flight mass spectra (points) and fits (lines) for (a) Sn and (b) Sn_2 mass peaks, taken from the spectrum in Figure 7. The fits demonstrate near-natural-abundance isotopic distributions.

component distribution, shown in Figure 11a, which gave peak arrival times of 39.2 and 75.7 μs, and a ratio of fast to slow component of ~2:1. The Sn_2 arrival-time distribution, shown in Figure 11b, was fit to a single-component distribution, since the small signal level made it difficult to discriminate between a single- and two-component distribution. The fit gave a peak arrival time of 66.3 μs. These values for Sn and Sn_2 correspond to most-probable speeds of 1.7×10^5 cm s^{-1} and 1.1×10^5 cm s^{-1}, peak KEs of 1.8 and 1.5 eV, and an equivalent temperature of 1.1×10^4 K, considering only the primary Sn component. The relative Sn:Sn_2 abundance determined as above is 3.5:1.0, an increase of 2.5 times over that at 532 nm.

C. Discussion. In examining our results and their implications for PLD-generated SnO_x films, we begin with the neutral composition and its wavelength dependence for the oxide target. At a subgap wavelength (532 nm), Sn_xO_x ($x = 1-3$) are the dominant ablation products. A marked change is observed at the near-gap (355 nm) wavelength, where the relative Sn:Sn_xO_y and SnO:Sn_2O_2 abundances increase and Sn is the dominant product. This is a key result of our work, which may signal a fundamental change in mechanism for the laser−target interaction, e.g., the onset of electronic processes. Alternatively, laser-induced processes in the gas phase may become important due to the higher photon energy and increased absorption. For example, 355 nm laser irradiation overlaps the strong $D^1\Pi \leftarrow X^1\Sigma^+$ system of SnO.[40] For both targets 355 nm ablation produces a higher yield of ionic products, observed as an increase in background signal. Mass-resolved detection of ablated ions should give additional insight into the origin of the wavelength dependence.

Results for the Sn target can be compared to studies at other wavelengths. Jackson et al.[41] observed Sn_x ($x = 1-7$) species using Fourier transform ion cyclotron resonance (ICR) mass spectrometry following 1064 nm ablation of tin foil at a intensity of 100 J cm^{-2}. Changes in the intensities of negative ion peaks

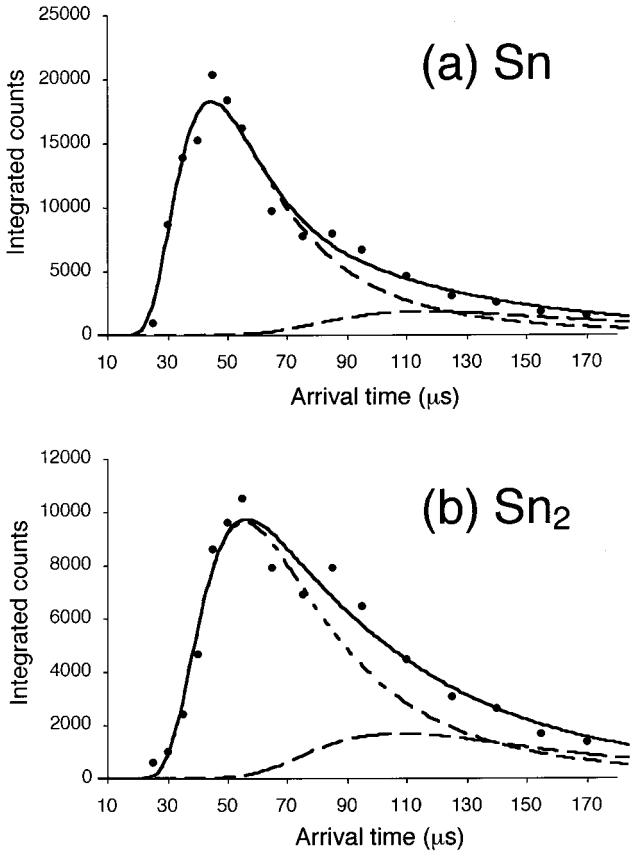

Figure 9. Arrival-time distributions (points) for (a) Sn and (b) Sn_2 from 532 nm ablation of Sn target. The distributions are bimodal and were fit to the sum of two unshifted time-transformed MB speed distributions. The solid line in each plot is the two-component fit, and the individual components are shown as dashed lines.

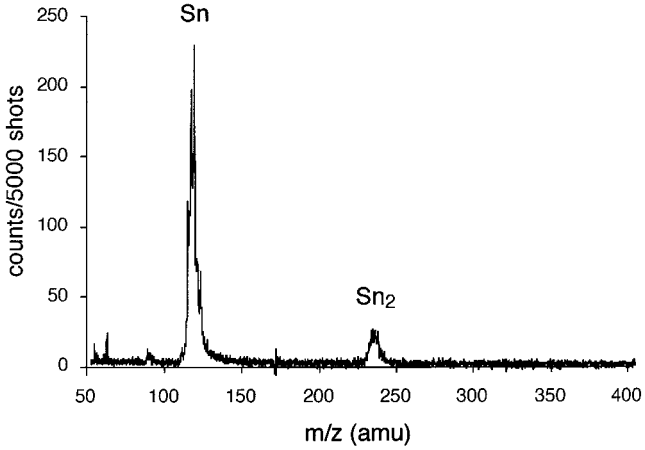

Figure 10. Mass spectrum of the neutral products of 355 nm pulsed laser ablation of a Sn target.

following flooding of the ICR cell with resonant electrons showed a significant population of neutral Sn_x ($x = 3-6$). In contrast, ablation at 248 nm was found to produce Sn, Sn^+, and some Sn^{2+} with no evidence of clusters.[37] These results in combination with ours reveal a consistent decrease in cluster yield at shorter wavelengths, which may result from laser-induced processes in the gas phase.

The KE distributions of ejected species from the oxide target are consistently MB-like. Typical most-probable speeds are (1−2) $\times 10^5$ cm s^{-1}, with peak KEs of 1−2 eV and temperatures of 10^4 K. The peak KEs exhibit little variation with wavelength, with the exception of atomic Sn ejected at 355 nm, which

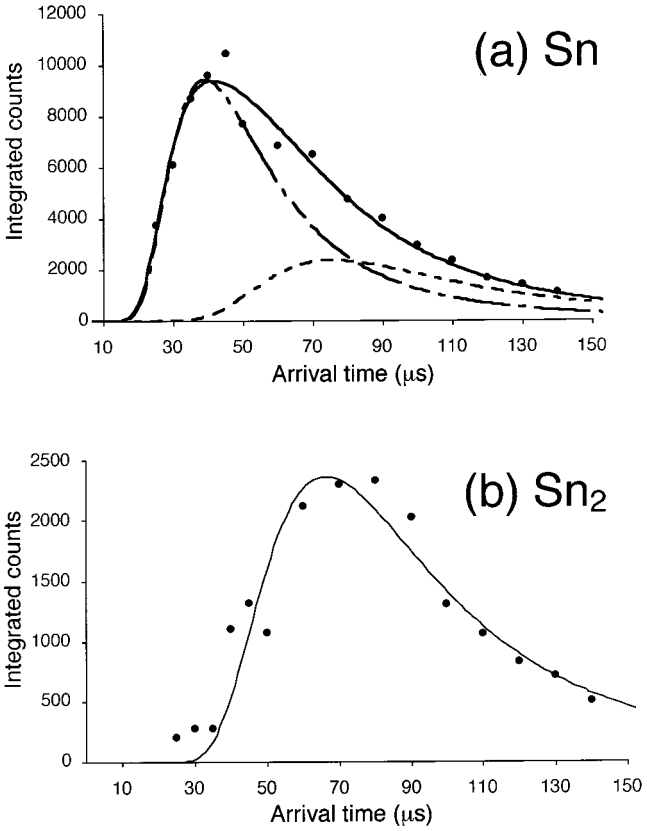

Figure 11. Neutral arrival-time distributions (points) for (a) Sn and (b) Sn_2 from 355 nm ablation of a Sn target. The Sn distribution was fit to a two-component MB distribution, while that for Sn_2 was fit to a single component distribution. The lines represent the fits following the notation used in Figure 9.

exhibits the highest most-probable speed of 2.2×10^5 cm s^{-1} and peak KE of 3 eV or temperature of $\approx 1.8 \times 10^4$ K. This may indicate that Sn is not a primary ablation product but originates from laser-induced processes in the gas phase (e.g., photodissociation of SnO monomers or clusters), a hypothesis supported by the dramatic increase in $Sn:Sn_xO_y$ at 355 nm. We note that agreement with a MB distribution is not evidence for a thermal mechanism. Studies of 248 nm laser desorption of Au from a metal target shows MB-like distributions, but with mean speeds that are inconsistent with a thermal model.[42,43] Moreover, Au produced at intensities near and above the ablation threshold also show MB-like distributions, suggesting that 10−20 collisions per particle are insufficient to impart a significant stream velocity.[42] Our inferred neutral angular dependence (Figure 4) also suggests the presence of gas-dynamic effects in a intensity regime where the arrival-time distributions are still MB-like.

Neutral species ejected from the metal target consistently exhibit bimodal MB distributions. Our results are qualitatively similar to those of Theim et al.,[32] who examined the speed distributions of neutral atoms from ablation of metal and compound targets at intensities below plasma threshold. Atomic Cu produced in 532 nm ablation from a Cu target at intensities of 10^8 W cm^{-2} exhibited an MB-like speed distribution corresponding to a temperature of 1.12×10^4 K, similar to that obtained here for atomic Sn from the metal target, while at higher intensities bimodal distributions were observed. This may reflect a hybrid electronic/thermal mechanism,[44] and indeed the influence of electronic processes in desorption from metals at low photon energies has recently been demonstrated.[45] The slow component may thus reflect thermal vaporization, or result from fragmentation of higher clusters (e.g., Sn_3) in the ionization step.

We next consider the specific implications of our results for PLD-generated SnO_x films. Vispute et al.[13] observed an oxygen-deficient SnO_x ($x < 2$) film produced in 694 nm PLD from an SnO_2 target under high vacuum conditions. Similarly, our results[19] show a reduced O:Sn stoichiometry of films grown at 532 nm which correlates with that of the neutral gas-phase Sn-containing products and indicates that the undetected oxygen is not ultimately incorporated into the deposited film. It was assumed in ref 13 that oxygen loss occurred at the target; however, we can draw no conclusions about this from our results.

Additional insight is gained from the work of Hu et al.,[12] who reported polycrystalline SnO_2 films of similar orientation and average grain size (4−5 nm) grown using 248 nm PLD from SnO_2 and Sn targets, followed in each case by postdeposition annealing in an oxygen atmosphere. Our results suggest that UV ablation of both types of targets produces primarily atomic Sn, at least for the neutral products, with similar energetics. Therefore, it is not surprising that similar as-grown films are produced by Hu et al. with metal and oxide targets. The broader implication of our work is that UV PLD from oxide targets may produce a more severe oxygen deficiency in the general case.

To date only one PLD study has reported the growth of polycrystalline *near-stoichiometric* (i.e., SnO_2) films on room-temperature substrates under high vacuum conditions,[16] where a wavelength of 1064 nm and energy densities of 20−150 J cm^{-2} were used. It may be that the trend we observe, an increase in oxygen content with increasing wavelength, continues to longer wavelength. Alternatively, the high intensities used may have led to stoichiometric deposition. Our preliminary studies at 532 nm do show a modest increase in yield of oxide species at higher intensity, but further studies are needed to sort out the influence of wavelength and intensity effects in producing the interesting result of ref 16. In general, the growth of polycrystalline SnO_2 films from either 532 or 355 nm PLD will require either postdeposition oxidation or reactive deposition in an oxygen atmosphere.

IV. Conclusions

We have probed neutral species generated in laser ablation of SnO_2 and Sn targets at both 532 and 355 nm and at intensities of 10^8 W cm^{-2}. For the oxide target, the major (>85%) Sn-containing species observed at 532 nm are of composition Sn_xO_x (x=1−3). The ratio of $Sn:Sn_xO_y$ species is increased by approximately 40 times for ablation at 355 nm, which may arise from the onset of electronic processes in the target or from laser-induced processes in the gas phase. The primary products of ablation from Sn targets at intensities near threshold are Sn and Sn_2, with an increase in the $Sn:Sn_2$ ratio of 2.5 times at the shorter wavelength.

The neutral arrival-time distributions for species ejected from the oxide target were well fit by unshifted time-transformed MB speed distributions, while those for species ejected from the metal target were consistently bimodal. The fits yield typical most-probable speeds of 10^5 cm s^{-1}, peak KEs of 1−2 eV, and temperatures of $\sim 10^4$ K. The observed KEs exhibit little variation with wavelength, with the exception of Sn ejected from the oxide target. The angular distribution of ejected neutrals inferred from analysis of the thickness distribution of amorphous SnO films deposited using 532 nm ablation from the oxide target gives sharpness parameters n of 6−15, indicating the presence

of gas-dynamic effects in a intensity regime where the arrival-time distributions are still MB-like.

Our results are helpful in understanding previous studies of PLD-generated SnO_x films, and illustrate the importance of fundamental characterization of pulsed laser ablation in understanding the properties of PLD films. However, a complete understanding of laser-induced particle emission from these targets should include the intensity dependence of neutral composition and energetics at different wavelengths, which will be important in deconvoluting wavelength and intensity effects. A detailed study of this will be the subject of a future report. We also plan to explore other parameters including ion composition and energetics, spectroscopic characterization of gas-phase species in the plume, and direct measurement of the angular distribution of neutral and ionic species.

Acknowledgment. S.A.R. acknowledges the National Science Foundation CAREER program (CHE-9702803), the Arnold and Mabel Beckman Foundation, the Marquette Center for Sensing Technology, and the Petroleum Research Fund administered by the American Chemical Society for partial support of this research, and thanks Binyong Liang and Jason P. Schmidt for assistance in construction and calibration of the experimental apparatus. F.J.L. acknowledges C. Pugh-Smith for assistance in the production of tin oxide targets and N. Schook for technical support. The authors acknowledge useful discussions with J. Hossenlopp and thank her for stimulating our interest in tin oxide films.

References and Notes

(1) Iida, H.; Shibata, N.; Mishuka, T.; Ito, A.; Karasawa, H.; Hayashi, Y. *IEEE Electron Device Lett.* **1983**, *EDL-4*, 157.
(2) Schroder, D. K. *IEEE Trans. Electron Devices* **1978**, *25*, 90.
(3) Göpel, W. *Sens. Actuators, B* **1994**, *18/19*, 1.
(4) Takahata, K. In *Chemical Sensor Technology*; Seiyama, T., Ed.; Elsevier: Amsterdam, 1988; p 39.
(5) Heiland, G. *Sens. Actuators* **1982**, *2*, 343.
(6) Semancik, S.; Fryberger, T. B. *Sens. Actuators, B* **1990**, *2*, 97.
(7) Sberveglieri, G.; Groppelli, S.; Nelli, P.; Camanzi, A. G. *Sens. Actuators, B* **1991**, *5*, 343.
(8) Kohl, D. *Sens. Actuators, B* **1990**, *1*, 158.
(9) Matsyshima, S.; Teraoka, Y.; Miura, N.; Yamazoe, N. *Jpn. J. Appl. Phys.* **1988**, *27*, 1798.
(10) Simianu, V. C.; Hossenlopp, J. M. *Appl. Organomet. Chem.* **1997**, *11*, 147.
(11) Serrini, P.; Briois, V.; Horrillo, M. C.; Traverse, A.; Manes, L. *Thin Solid Films* **1997**, *304*, 113.
(12) Hu, W. S.; Liu, Z. G.; Wu, Z. C.; Feng, D. *Mater. Lett.* **1996**, *28*, 369.
(13) Vispute, R. D.; Godbole, V. P.; Chaudhari, S. M.; Kanetkar, S. M.; Ogale, S. B. *J. Mater. Res.* **1988**, *3*, 1180.
(14) Godbole, V. P.; Vispute, R. D.; Chaudhari, S. M.; Kanetkar, S. M.; Ogale, S. B. *J. Mater. Res.* **1990**, *5*, 372.
(15) Lal, R.; Grover, R.; Vispute, R. D.; Viswanathan, R.; Godbole, V. P.; Ogale, S. B. *Thin Solid Films* **1991**, *206*, 88.
(16) Dai, C. M.; Su, C. S.; Chuu, D. S. *Appl. Phys. Lett.* **1990**, *57*, 1879.
(17) Morosova, N. V.; Gas'kov, A. M.; Kuznetsova, T. A.; Putilin, F. N.; Rumyantseva, M. N.; Shatnov, V. I. *Inorg. Mater.* **1996**, *32*, 292.
(18) Hu, W. S.; Liu, Z. G.; Zheng, J. G.; Hu, X. B.; Guo, X. L.; Göpel, W. *J. Mater. Sci. Mater. Elec.* **1997**, *8*, 155.
(19) Lamelas, F. J.; Reid, S. A. *Phys. Rev. B* **1999**, *60*, 9347.
(20) Reid, S. A. *Chem. Phys. Lett.* **1999**, *301*, 517.
(21) See, e.g.: *Pulsed Laser Deposition of Thin Films*; Chrisey, D. B., Hubler, G. K., Eds.; Wiley: New York, 1994.
(22) Lowndes, D. H. In *Laser Ablation and Desorption*; Miller, J. C., Haglund, R. F., Jr., Eds.; Academic: San Diego, 1998.
(23) See, e.g.: (a) *Laser Ablation: Principles and Applications*; Miller J. C., Ed.; Springer-Verlag: Berlin, 1994. (b) *Laser Ablation: Mechanisms and Applications—II*; Miller, J. C., Geohegan, D. B., Eds.; AIP: New York, 1994.
(24) Haglund, R. F., Jr.; Itoh, N. In *Laser Ablation: Principles and Applications*; Miller J. C., Ed.; Springer-Verlag: Berlin, 1994.
(25) Gill, C. G.; Allen, T. M.; Anderson, J. E.; Taylor, T. N.; Kelly, P. B.; Nogar, N. S. *Appl. Opt.* **1996**, *35*, 2069.
(26) See, e.g.: Wang, S. L., Ledingham, K. W. D.; Singhal, R. P. *J. Phys. Chem.* **1996**, *100*, 11282, and references therein.
(27) Radzig, A. A.; Smirnov, B. M. *Reference Data on Atoms, Molecules, and Ions;* Springer-Verlag: Berlin, 1985.
(28) Colin, R.; Drowart, J.; Verhaegen, A. G. *Trans. Faraday Soc.* **1965**, *61*, 1364.
(29) Zimmermann, E.; Königs, S.; Neuschütz, D. *Z. Phys. Chem.* **1996**, *193*, 195.
(30) van Ingen, R. P. *J. Appl. Phys.* **1996**, *79*, 467.
(31) Anderson, J. B.; Andres, R. P.; Fenn, J. B. *Adv. Chem. Phys.* **1966**, *10*, 175.
(32) Thiem, T. L.; Watson, L. R.; Dressler, R. A.; Salter, R. H.; Murad, E. *J. Phys. Chem.* **1994**, *98*, 11931.
(33) Utterback, N. G.; Tang, S. P.; Friichtenicht, J. F. *Phys. Fluids* **1976**, *19*, 900.
(34) Namiki, A.; Kawai, T.; Ichige, K. *Surf. Sci.* **1986**, *166*, 129.
(35) Zheng, J. P.; Huang, Z. Q.; Shaw, D. T.; Kwok, H. S. *Appl. Phys. Lett.* **1989**, *54*, 280.
(36) Kools, J. C. S.; Baler, T. S.; De Zwart, S. T., Dieleman, J. *J. Appl. Phys.* **1992**, *71*, 4547.
(37) Timm, R.; Willmott, P. R.; Huber, J. R. *J. Appl. Phys.* **1996**, *80*, 1794.
(38) Jenkins, F. A.; White, H. E. *Fundamentals of Optics*; McGraw-Hill: New York, 1950; pp 254—278.
(39) Saenger, K. L. In *Pulsed Laser Deposition of Thin Films*; Chrisey, D. B., Hubler, G. K., Eds.; Wiley: New York, 1994.
(40) Dube, P. S.; Rai, D. K. *J. Phys. B: At. Mol. Phys.* **1971**, *4*, 579.
(41) Jackson, P.; Dance, I. G.; Fisher, K. J.; Willett, G. D.; Gadd, G. E. *Int. J. Mass Spectrom. Ion Processes* **1996**, *157/158*, 329, and references therein.
(42) Bennett, T. D.; Grigoropoulos, C. P.; Krajnovich, D. J. *J. Appl. Phys.* **1995**, *102*, 726.
(43) Bennett, T. D.; Krajnovich, D. J.; Grigoropoulos, C. P. *Phys. Rev. Lett.* **1996**, *76*, 1659.
(44) See, e.g.: Lee, I.; Callcott, T. A.; Arakawa, E. T. *Phys. Rev. B* **1993**, *47*, 6661.
(45) Hoheisel, W.; Vollmer, M.; Träger, F. *Phys. Rev. B* **1993**, *48*, 17463.